

Selective Crystalline Seed Layer Assisted Growth of Vertically Aligned MgZnO Nanowires and Their High-Brightness Field-Emission Behavior

Dong Chan Kim, Bo Hyun Kong, Sanjay Kumar Mohanta, Hyung Koun Cho,*
Jae Hong Park, and Ji Beom Yoo

*School of Advanced Materials Science and Engineering, Sungkyunkwan University,
300 Cheoncheon-dong, Jangan-gu, Suwon, Gyeonggi-do, 440-746, Korea*

Received January 8, 2009; Revised Manuscript Received July 9, 2009

ABSTRACT: This article reports a new approach for fabricating vertically aligned MgZnO nanowire arrays using selective crystalline seed layers deposited at relatively high temperatures by metalorganic chemical vapor deposition. In the phase-separated MgZnO seed layers, Zn-rich regions with a wurtzite structure allowed the growth of slim MgZnO nanowires, while the Mg-rich seeds with a cubic or amorphous-like structure hindered the formation of nanowires. The photoluminescence of these nanowires showed a remarkable increase in the activation energy of the excitons, ~100 meV. The field-emission performance showed excellent emission behavior with extremely improved brightness, ~80 times higher current density than that of the ZnO nanowires grown under the same conditions. Models for the growth evolution of slim nanowires on Si substrates were also proposed, based on microstructural characterization.

1. Introduction

The synthesis of low-dimensional nanostructures in various forms has attracted considerable technological and scientific interest due to the physical and optical properties and the discovery of new physical meaning induced by the quantum-confinement effect.^{1,2} One-dimensional (1D) ZnO nanostructures (i.e., nanowires, nanorods, nanobelts, nanorings, etc.) have been the subject of intense research for applications in short-wavelength light-emitting devices and ultraviolet field emitters on account of their wide bandgap and high exciton binding energy, which can allow the production of devices with their performance unaffected by temperature.^{3,4} Vertically aligned ZnO nanowire arrays are more suitable structures for the fabrication of electronic devices, considering the interconnection of a metal layer and the feasibility of integration processes.^{5,6} The ZnO nanowires-based field emitters are expected to have a longer lifetime than carbon-based field emitters due to the chemical and environmental stability of oxide materials. Although many techniques have been used to synthesize vertically well-aligned ZnO nanowire arrays,^{5–9} metalorganic chemical vapor deposition (MOCVD) has been demonstrated to be a promising tool with particular advantages of accurate doping, low-temperature, catalyst-free epitaxial growth, etc.^{9–11} However, this method produces dense and broad ZnO nanowires (> 50 nm). Moreover, although the nanowires are highly crystalline with excellent optical quality, it is difficult to control the density and tip shape of the nanowires, which has a detrimental effect on the performance of field emitters due to the blunt tip shape and electric arcing. Therefore, the low emission intensity of ZnO-based field emitters and the difficulty in obtaining vertically aligned ZnO nanowire arrays with a narrower shape without the use of metal catalysts has limited field-emission applications to carbon nanotubes (CNTs).^{12,13} In this context, the incorporation of a small quantity of Mg atoms in the ZnO matrix can

enhance the emission efficiency,^{14,15} and an increase in synthesis temperature can improve the crystalline quality and luminescence intensity.¹⁶ Therefore, it is believed that both the addition of a small quantity Mg and the synthesis of vertically aligned nanowire arrays with the appropriate density at high temperatures will lead to significant improvement in the field-emission behavior. This paper reports a method for synthesizing very slim, vertically aligned single crystalline MgZnO nanowire arrays by growing small wurtzite crystalline Zn-rich phases selectively at high temperatures by MOCVD. The nanowires showed tremendous improvement in emission behavior due to the high crystalline quality and vertical alignment of nanowire arrays with the appropriate density at high growth temperatures. The detailed growth mechanism for these vertically aligned MgZnO nanowire arrays based on the microstructural characterizations is also presented.

2. Experimental Section

1D MgZnO nanowires were grown on Si substrates using a low-pressure MOCVD method, with diethylzinc (DEZn, purity 99.9995%), bis-cyclopentadienyl-magnesium (Cp₂Mg, purity 99.999%), and pure oxygen gas (O₂, purity 99.999%) as the reactive gases. Argon was used as the carrier gas. All Si substrates were degreased in an ultrasonic bath with acetone, ethanol, and deionized water for 5 min each. The Cp₂Mg flow rate during the growth of MgZnO nanowires was 1.4 μmol/min, while the DEZn flow rates was kept constant at 6.1 μmol/min. The nanowires were grown at temperatures ranging from 450–500 °C with a reactor pressure of 1 Torr for 30 min. No buffer layers or metal catalysts were required to produce the vertically aligned nanowires in this MOCVD method. The maximum level of Mg incorporation in the ZnO that allows the synthesis of vertically aligned nanowires under these growth conditions was approximately ~8 at %. The ZnO nanowires were also grown for comparison.

The morphology of the fabricated nanowires was observed by field-emission scanning electron microscopy (FESEM, JSM6700F). The microstructure was examined by transmission electron microscopy (TEM, JEM 3010) and high-resolution TEM operated at 300 kV. The TEM specimens were prepared by mechanical polishing and ion-milling at a low current Ar⁺ ion dose to prevent deformation during

*To whom correspondence should be addressed. E-mail: chohk@skku.edu.

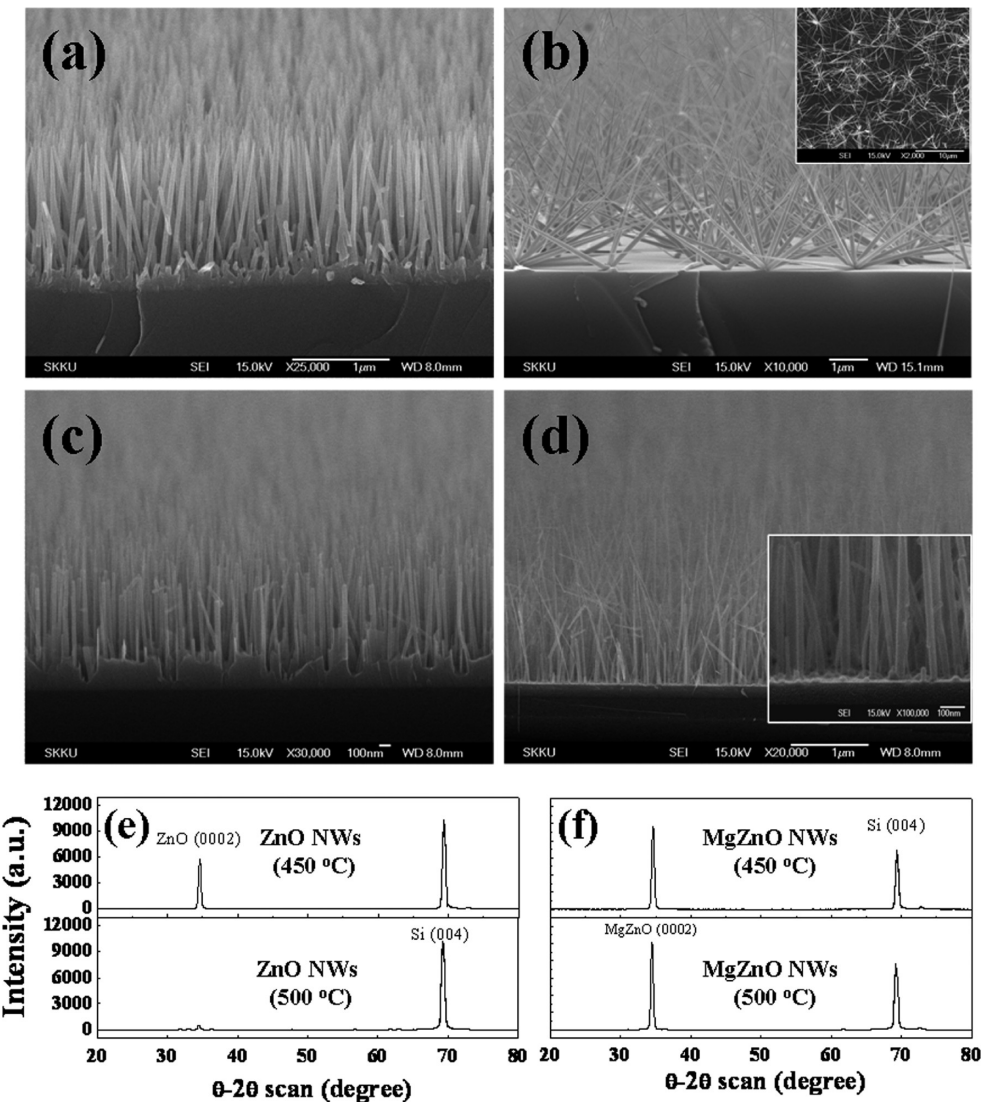


Figure 1. Cross-sectional FESEM images of ZnO [(a) and (b)] and MgZnO [(c) and (d)] nanowires grown at 450 and 500 °C. The insets in (b) and (d) show the plane-view FESEM image of ZnO multipod nanostructures and magnified FESEM image of MgZnO nanowire arrays, respectively. Panels (e) and (f) θ - 2θ XRD curves of ZnO and MgZnO nanowires grown on Si substrates at 450 and 500 °C, respectively, where the y-axis scale is the same.

ion-milling. Energy dispersive X-ray fluorescence (EDX) analysis was carried out during the TEM observations with a nanobeam to probe the distribution of Mg atoms in the MgZnO nanowires. Variable temperature photoluminescence (PL) measurements were performed by placing the samples inside a closed cycle He cryostat and using 325 nm He–Cd laser as the excitation source. The room temperature field-emission (FE) measurements were performed in a high vacuum chamber at a base pressure of 8×10^{-7} Torr. The distance between the electrodes was approximately 200 μ m, while the sample size was 15 \times 15 mm².

3. Results and Discussion

Figure 1 shows FESEM images of the 1D ZnO and MgZnO nanostructures synthesized on Si substrates at different temperatures (450–500 °C). The ZnO nanowires become more slender and randomly inclined on the Si surface with increasing growth temperature (Figure 1a,b). At the highest growth temperature of 500 °C, most of the nanowires contained many branches from the less dense seeds, and appeared to be multipod nanostructures. Several studies have reported that ZnO nanowires form in the presence of a two-dimensional (2D) interfacial layer between the nanowires and substrate.^{9,17}

In the present case, the vertically aligned ZnO nanowires grown at 450 °C had an interfacial layer, while the inclined nanowires observed at 500 °C showed no sign of the formation of an interfacial layer. In the case of Mg incorporated nanowires, the width of the MgZnO nanowires were narrower than that of ZnO. FESEM showed that the MgZnO nanowires grown at high temperatures were vertically well-aligned with a small inclination (Figure 1d). The length and diameter of the MgZnO nanowires grown at 500 °C were 2.8–3.0 μ m and ~10 nm, respectively. Figure 1e,f shows the θ - 2θ XRD patterns of the 1D ZnO and MgZnO nanostructures grown directly on the Si substrates at 450–500 °C. These ZnO and MgZnO nanowires showed a highly preferred orientation along the *c*-axis. However, the ZnO nanowires grown at 500 °C showed a lower $I_{\text{ZnO}(0002)}/I_{\text{Si}(100)}$ intensity ratio, which was attributed to the random inclination and reduced density of nanowires. On the other hand, the MgZnO nanowires grown at the same temperature showed a considerably enhanced $I_{\text{MgZnO}(0002)}/I_{\text{Si}(100)}$ intensity ratio, highlighting the vertical alignment and high crystalline quality. The dominant diffraction peaks at 34.5° correspond to the (0002) plane of a

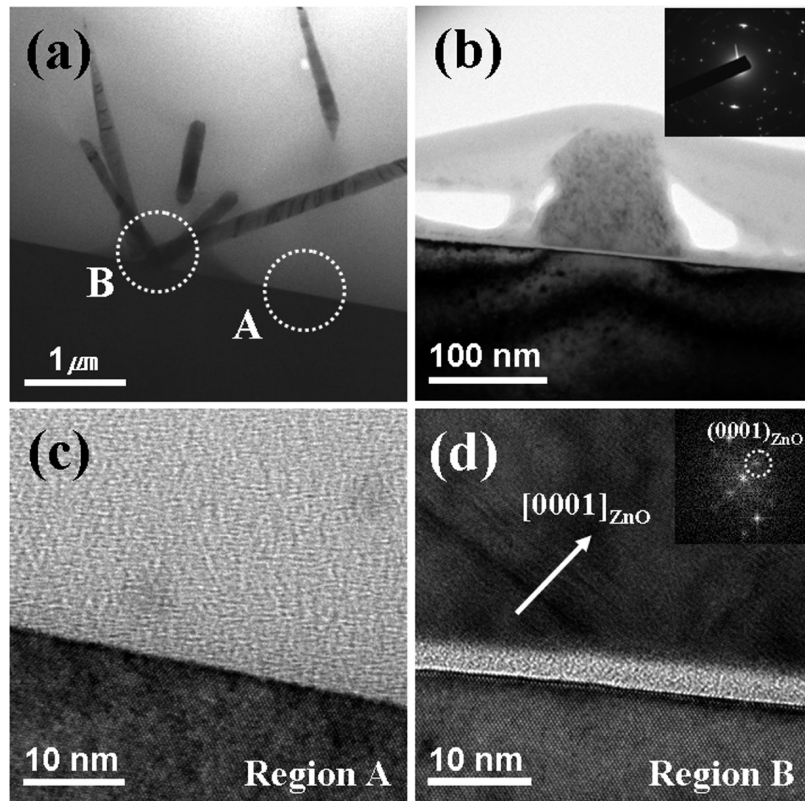


Figure 2. Cross-sectional TEM images of ZnO nanowires grown at 500 °C: (a) low magnification image showing multipod nanostructures, (b) the seed layer of a multipod nanostructure showing polycrystalline nature, (c) HRTEM image from the region without an interfacial layer, and (d) HRTEM image from the seed layer of a multipod nanostructure. The insets show the DPs revealing the crystal structure.

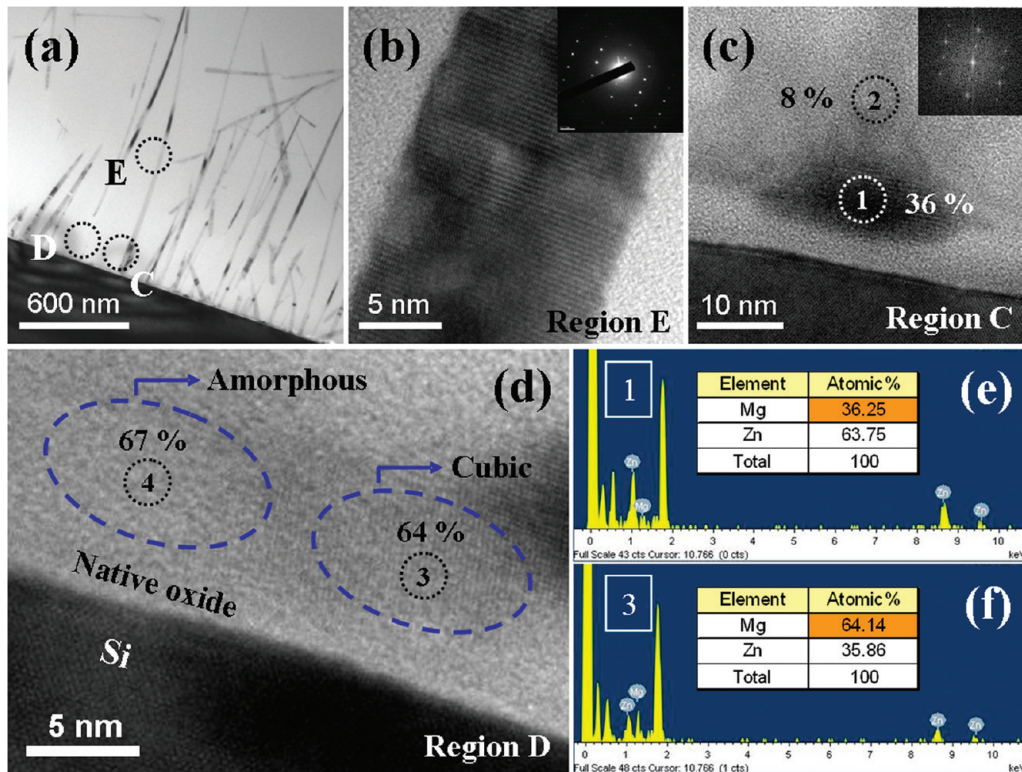


Figure 3. Cross-sectional TEM images and EDX spectra of the MgZnO nanowires grown at 500 °C: (a) low magnification image showing vertical alignment, (b) HRTEM image of a nanowire (c) HRTEM image of the seed layer of a nanowire showing wurtzite structure, and (d) HRTEM image from the region without nanowires. The insets show the DPs revealing the wurtzite crystal structures. The EDX scan results from (e) the seed region of the nanowire and (f) without nanowires.

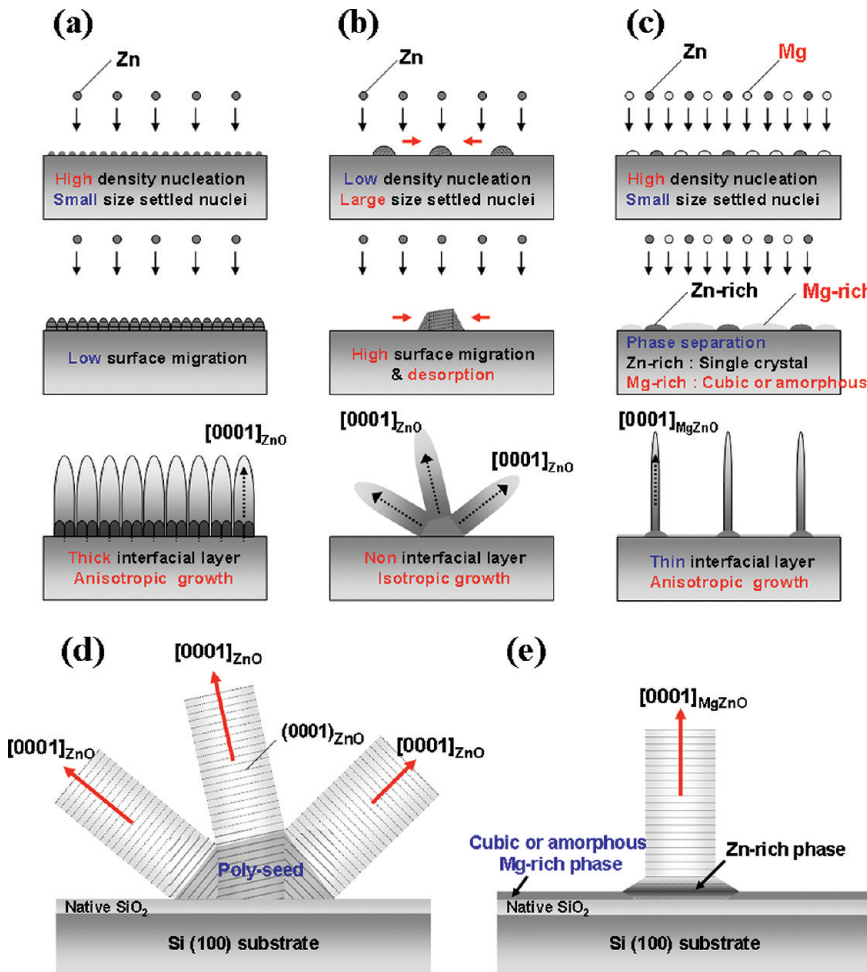


Figure 4. Schematic models on the growth evolution of (a) vertically aligned ZnO nanowires grown at relatively low temperature (ref 9), (b) ZnO multipod nanostructures, and (c) vertically aligned MgZnO nanowires grown at high temperatures. More detailed schematic diagrams of the growth of (d) ZnO multipod nanostructures and (e) vertically aligned MgZnO nanowires grown at high temperatures. The lines indicate the (0002)_{ZnO} plane.

wurtzite ZnO and MgZnO crystal. To the best of our knowledge, this width is the narrowest among the vertically aligned nanowires fabricated by MOCVD. The formation of vertically aligned nanostructures with a narrow tip shape, which can be obtained at high processing temperatures, is suitable for applications as high efficiency field emitters in field-emission displays (FEDs).^{18,19} However, the results show that even though an increase in growth temperature allows the production of single crystal ZnO nanowires with high crystalline quality, inclination of the nanowires occurred at higher growth temperature (Figure 1b). Therefore, there is a limit for the realization of vertically aligned and slim ZnO nanowires by increasing the growth temperature. Interestingly, the incorporation of Mg atoms in the ZnO nanowires leads to the formation of vertically aligned nanowires at a relatively high growth temperature, as shown in Figure 1d.

TEM and HRTEM were used to characterize the microstructural behavior on the incorporation of Mg in the nanowires grown at 500 °C. Figures 2 and 3 show TEM images of the inclined ZnO nanowires and vertically aligned MgZnO nanowires, respectively, grown at the same temperature. Dense ZnO multipod structures with many nanowires originating from the same seed were formed at higher synthesis temperatures (Figure 2a). The seed of the multipod contained large grains, approximately 142 nm in width (Figure 2b). No

2D thin films were actually deposited on the substrate surface, as shown in Figure 2c. The magnified HRTEM image of the seeds shows a polycrystalline behavior with a random alignment of (0002)_{ZnO} planes (Figure 2d). On the other hand, MgZnO nanowires grown at 500 °C showed good vertical alignment, despite being very slim and grown at high temperatures (Figure 3a). The HRTEM image and diffraction patterns (DPs) of a vertically aligned MgZnO nanowire revealed the nanowires to be single crystal wurtzite structures with a *c*-axis preferred orientation, that is, along the [0002] direction (Figure 3b). The seeds of the MgZnO nanowires were 20 nm in diameter and exhibited a single crystal wurtzite structure with a *c*-axis preferred orientation, as shown in Figure 3c. Therefore, the seeds in both ZnO and MgZnO nanowires act as templates on the growth of the respective nanowires. Because all ZnO based nanowires were grown with a *c*-axis preferred orientation, the ZnO on the polycrystalline seeds led to the formation of ZnO multipod structures, while the MgZnO on single crystal seeds resulted in the formation of vertically aligned MgZnO nanowires. On the other hand, the Si substrate surface, where nanowires were not formed, showed a slightly different contrast, as shown in Figure 3d. This region consists of a native silicon dioxide layer and a thin layer with a 5 nm thickness. A part of the thin layer showed lattice fringes or atomic images indicating a crystal, and the

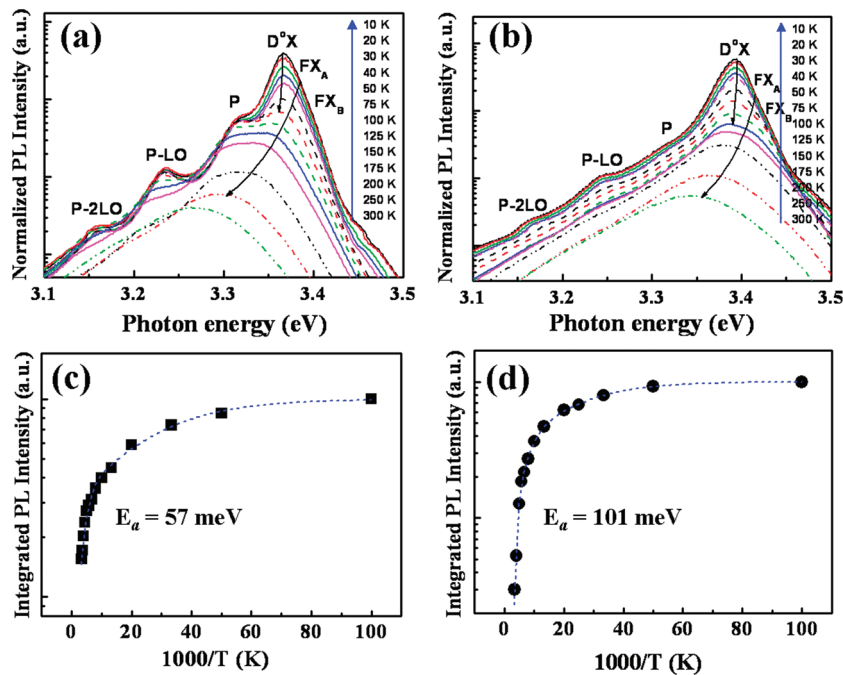


Figure 5. Temperature-dependent PL spectra of (a) ZnO and (b) MgZnO nanowires grown at 500 °C. The integrated PL intensities as a function of $1000/T$ for (c) ZnO and (d) MgZnO nanowires grown at 500 °C.

other showed an amorphous-like image. Interestingly, these crystals had a cubic structure not a wurtzite structure. Therefore, the formation of vertically well aligned nanowires with a single crystal wurtzite structure was attributed to the small islands with a wurtzite structure embedded in the cubic or amorphous structure matrix during the initial stages of growth. Furthermore, Figure 3e,f shows EDX point scans of the distribution of Mg atoms on different regions of the MgZnO nanowires. The Mg content in the seed layer with a wurtzite structure was relatively high, 36 at % (Figure 3c,e), while the average Mg composition in the body of the MgZnO nanowire was approximately ~8 at %, where the Mg composition in the body of the MgZnO nanowire is uniform along the nanowires with the deviation of below 1% except the seed region. According to previous reports, the Mg composition of ~36 at % might be the maximum value showing MgZnO with a stable wurtzite structure, while the theoretical solubility limit is only 4 at %.^{20,21} Furthermore, the thin layers formed in the region containing no nanowires on the Si surface have a remarkably high Mg composition (≥ 60 at %) with a cubic phase structure (Figure 3d,f). Earlier, it was also reported that the MgZnO layers containing more than 60 at % Mg formed a cubic phase, which is consistent with our observations.^{22,23} The Mg-rich cubic or amorphous-like regions at the initial stage did not form nanowires in continuous growth due to the suppression of the wurtzite structure nanowires.

Considering the microstructural behaviors and Mg distribution in the nanowires, schematic growth models were proposed to explain the growth evolution of the vertically aligned MgZnO nanowires and the ZnO multipod nanostructures on the Si substrates at high processing temperatures, as demonstrated in Figure 4. A recent study proposed a growth model for vertically aligned ZnO nanorods in the presence of the interfacial layer, in which the defects observed in the interfacial layer play a key role in nanorod growth (Figure 4a).⁹ In general, three-dimensional island growth is desirable in heterostructures with large lattice mismatch, such

as ZnO/Si substrates, which leads to a decrease in contact area. In addition, based on the conventional nucleation and growth model, an increase in growth temperature promotes surface migration of the as-deposited atoms resulting in the agglomeration of the nucleated islands, as shown in Figure 4b.²⁴ The agglomerated islands contain several grains with different orientations from each other, and the deposition of ZnO nanowires proceeds along the *c*-axis crystal orientation of the seed layer to form ZnO multipod nanostructures (Figure 4d). In contrast, MgZnO nanowires with vertical alignment and a high aspect ratio were synthesized with the assistance of small size wurtzite islands (Figure 4c). At the initial stage, Mg incorporation in ZnO is expected to disturb the surface migration of the as-deposited atoms due to the relatively high adsorption energy of Mg metal adatoms.²⁵ Several groups reported that the MgZnO alloy with a high Mg composition showed phase separation into wurtzite Zn-rich and rocksalt Mg-rich phases under thermal equilibrium conditions due to the thermodynamic solubility limit of Mg in ZnO.^{22,23} These reports are consistent with the present results showing the formation of thin MgZnO layers with a cubic or amorphous-like Mg-rich phase and a wurtzite Zn-rich phase at the initial stages of growth, as shown in Figures 3 and 4c. After forming the seed layers, wurtzite phase MgZnO nanowires with ~8% Mg formed selectively on the wurtzite seed and grew vertically on the Si substrates, as shown in Figure 4e.

Furthermore, temperature-dependent PL and field-emission measurements were carried out to compare the emission behavior of the ZnO and MgZnO nanowires grown at 500 °C. Figure 5 shows the temperature-dependent PL spectra and integrated PL intensity of the ZnO and MgZnO nanowires as a function of temperature. At 10 K, the PL spectrum from the ZnO multipod nanostructures was dominated by emission lines corresponding to donor bound exciton (D^0X at 3.3665 eV) (Figure 5a).²⁶ The small asymmetry of the PL band on the high energy side of D^0X was attributed to the presence of the A- and B-valence band (X_A and X_B) of free-exciton emission

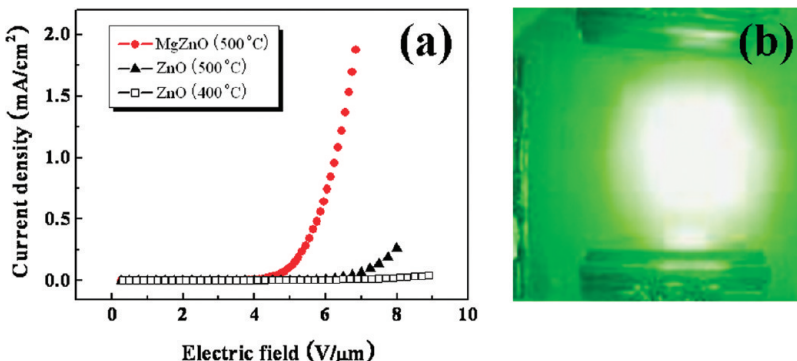


Figure 6. (a) Field-emission J-E plot from the ZnO nanowires grown at 400 and 500 °C and MgZnO nanowires grown at 500 °C on Si substrates. (b) Electron emission image of the MgZnO nanowires at an applied electric field around 6 V/μm, showing homogeneous surface emission with significantly improved brightness.

and their excited states transitions.^{27,28} The PL spectrum also shows a broad low energy shoulder at around 3.314 eV (leveled as “P”) along with its LO phonon replicas at 3.238 and 3.167 eV with an energy separation of 76 and 147 meV, respectively. The P line can be resolved into two-electron satellites, a donor-to-acceptor pair, exciton–exciton scattering, and LO-phonon replicas of FX and D⁰X. With increasing temperature, the intensity of D⁰X decreases whereas that of FX increases and becomes dominant above 100 K due to the thermal dissociation of the bound exciton to free exciton at higher temperature. The PL spectrum at room temperature shows the exciton emission from the ZnO nanowires with a peak position at 3.27 eV. In contrast to ZnO, the PL spectra of the MgZnO nanowires show a blue shift in the near-band-edge excitonic emissions, as shown in Figure 5b. The 10 K PL spectrum from the MgZnO nanorods is dominated by emission lines corresponding to donor bound exciton (D⁰X) at 3.393 eV and P line (at 3.323 eV), and its phonon replicas at 3.246 and 3.171 eV. The PL spectrum from the MgZnO nanowires at room temperature shows exciton emission with a peak at 3.345 eV. Hence, there was a blue shift of 75 meV in the room-temperature PL spectrum of MgZnO nanowires when compared to ZnO nanowires. It was reported that the exciton transition energy (E_{ex}) of MgZnO varies with Mg content in accordance with $E(Mg_xZn_{1-x}O) = E(ZnO) + 1.64 \times x$ [eV].²⁹ From this equation, the estimated Mg content in the MgZnO nanowires with an emission energy of 3.53 eV was ~ 5 at %, which is close to the value estimated by EDX. The PL peak shift can also be associated with laser heating or stress/strain in the film.^{30,31} No shift in the PL peak position due to laser heating was expected because the laser power was kept very low (< 3 mW) during the PL measurement. As different acquisition times may cause a peak shift under prolonged laser irradiation, the acquisition time of all spectra were also kept constant. Furthermore, the length of the MgZnO nanowires were 2.8–3.0 μm, and the penetration depth of the laser light at 325 nm was 60–120 nm. Therefore, the observed PL emission originates from the top region of the MgZnO nanowires only, and the top of the nanorods is expected to be stress free. Therefore, the observed blue-shift from the MgZnO nanowires is not believed to be related to the stress effect, but to Mg incorporation in ZnO. Figure 5b showed the decrease in the contribution of the LO phonon to the emissions spectra of MgZnO nanowires compared to ZnO multipod nanostructures, indicating a reduction in the coupling strength of the exciton–phonon interaction with Mg incorporation. Polar semiconductors experience a strong Frohlich

electron–phonon interaction that gives rise to an exciton-LO phonon interaction. Recently, Pan et al.²⁸ have reported a decrease in exciton-LO phonon coupling strength with increasing Mg content in MgZnO nanocrystals. Earlier, Wang et al.³² extracted the exciton-LO phonon coupling parameter of ZnO nanowires by resonant Raman scattering, and found that coupling strength decreases with decreasing nanowire diameter. Thus, the reduction of the exciton-LO phonon coupling strength of MgZnO nanowires compared to ZnO multipod nanostructures is due to the combined effect of Mg incorporation in ZnO and the decrease in nanowire diameter. The thermal activation energy (E_a) of ZnO and MgZnO nanowires were calculated from the Arrhenius plot of the PL results showing the behavior of the integrated intensity as a function of temperature (Figure 5c,d). The activation energy related to the high temperature regime for ZnO and MgZnO nanowires were approximately 57 and 101 meV, respectively. This activation energy for ZnO nanowires is similar to the binding energy of the free exciton (59 meV). In contrast, the activation energy for the MgZnO nanowires increased with the slow quenching of the integrated intensity with increasing temperature when compared to ZnO. This suggests that the free excitons can survive at relatively high temperatures, and it is expected to have stable device operation at high temperatures. The increase in activation energy in MgZnO nanowires was attributed to the larger impurity binding energy or carrier/exciton localization energy with Mg incorporation. Recently, Wassner et al. observed a relatively higher activation energy of 127 meV for MgZnO thin films with Mg contents $x = 0.37$.³³ In addition, the MgZnO films showed a relatively higher activation energy due to the carrier localization effect from phase separation.¹⁴ However, in this case, the observed PL emission originated mainly from the top region of the MgZnO nanowires. Therefore, an increase in activation energy due to the quantum confinement effect cannot be excluded in such slim nanowires with a diameter < 20 nm.

The field-emission results for ZnO and MgZnO nanowires synthesized at 500 °C are shown in Figure 6. Interestingly, the FE characteristics obtained from the MgZnO nanowires in this study are much better than those reported previously for MOCVD grown ZnO nanowires,¹⁸ even though the ZnO nanowires grown at 500 °C also showed a slightly higher emission current density. Despite the random alignment of the ZnO nanowires, the improvement in the FE characteristics of the samples synthesized at 500 °C was attributed to the better crystallinity of the nanowires at high temperatures. From the J vs E curves, the turn-on fields defined as the electric field

corresponding to a current density of $0.1 \mu\text{A}/\text{cm}^2$ were 3.8 and $2.7 \text{ V}/\mu\text{m}$ for the ZnO and MgZnO nanowires synthesized at 500°C , respectively (Figure 6a). However, the most remarkable difference in the FE results is the current density. At $6 \text{ V}/\mu\text{m}$, the MgZnO nanowires with vertical alignment and a narrow width showed a current density approximately 80 times higher than that of the ZnO nanowires. The electric field required for a current density of $1 \text{ mA}/\text{cm}^2$ is approximately $6 \text{ V}/\mu\text{m}$, which corresponds to the minimum emission current density for the operation of a video graphics array FED. Moreover, the Si integration process can be utilized with these vertically aligned MgZnO nanowire arrays on large size Si substrates. This tremendous increase in the FE characteristics was attributed to the simultaneous achievement of the improved crystalline quality at high-temperatures, and vertical alignment of the nanowire arrays with the appropriate density. Figure 6b shows an electron emission image of the transparent anode at an applied electric field of approximately $6 \text{ V}/\mu\text{m}$ during the FE measurement. This suggests that the entire surface emission is remarkably bright and homogeneous.

4. Conclusions

In summary, we have successfully realized the high-brightness field-emission performance from the vertically aligned and slim MgZnO nanowire arrays synthesized by MOCVD at a relatively high temperature of 500°C . The evolution of the vertically aligned MgZnO nanowires at higher growth temperatures was attributed to the formation of small size selective crystalline seeds with a wurtzite structure, which acted as a template for nanowire growth. In contrast, ZnO nanowires grown at high temperatures showed multipod nanostructures with nanowires originating from large size polycrystalline grains. The temperature-dependent PL results from the vertically aligned MgZnO nanowires revealed the slow quenching of exciton-related emission with a thermal activation energy of $\sim 101 \text{ meV}$, which allows stable device operation at high temperatures. The remarkable increase in the emission intensity of the MgZnO nanowires (~ 80 times higher than ZnO nanowires) was attributed to the achievement of high crystalline quality and vertically aligned slim nanowires with the appropriate density. On the basis of microstructural characterization, growth models were proposed to explain the growth evolution of slim nanowires on a Si substrate.

Acknowledgment. This work was supported by the KRF Grant (KRF-2007-521-D00191) and Grant No. the Korea Science and Engineering Foundation (KOSEF) grant funded by the Korea government (MEST) (No. 2009-0078876). This research was also financially supported by the Ministry of Knowledge Economy (MKE) and Korea Industrial Technology Foundation (KOTEF) through the Human Resource Training Project for Strategic Technology.

References

- Pavesi, L.; Negro, D. L.; Mazzoleni, C.; Franzo, G.; Priolo, F. *Nature* **2000**, *408*, 440.
- Jiang, X.; Xiong, Q.; Nam, S.; Qian, F.; Li, Y.; Lieber, C. M. *Nano Lett.* **2007**, *7*, 3214.
- Kong, X. Y.; Wang, Z. L. *Nano Lett.* **2003**, *3*, 1625.
- Wu, J. J.; Liu, S. C. *Adv. Mater.* **2002**, *14*, 215.
- Park, W. I.; Yi, G. -C. *Adv. Mater.* **2004**, *16*, 87.
- Sun, X. W.; Huang, J. Z.; Wang, J. X.; Xu, Z. *Nano Lett.* **2008**, *8*, 1219.
- Nobis, T.; Kaidashev, E. M.; Rahm, A.; Lorenz, M.; Lenzner, J.; Grundmann, M. *Nano Lett.* **2004**, *4*, 797.
- Huang, M. H.; Mao, S.; Feick, H.; Yan, H.; Wu, Y.; Kind, H.; Weber, E.; Russo, R.; Yang, P. *Science* **2001**, *292*, 1897.
- Park, D. J.; Lee, J. Y.; Kim, D. C.; Mohanta, S. K.; Cho, H. K. *Appl. Phys. Lett.* **2007**, *91*, 143115.
- Gruber, Th.; Kirchner, C.; Kling, R.; Reuss, F.; Waag, A. *Appl. Phys. Lett.* **2004**, *84*, 5359.
- Zhang, B. P.; Bihm, N. T.; Wakatsuki, K.; Liu, C. Y.; Segawa, Y.; Usami, N. *Appl. Phys. Lett.* **2005**, *86*, 032105.
- Wang, M. S.; Peng, L. M.; Wang, J. Y.; Chen, Q. *J. Phys. Chem. B* **2005**, *109*, 110.
- Jung, S. M.; Hahn, J.; Jung, H. Y.; Suh, J. S. *Nano Lett.* **2006**, *6*, 1569.
- Shibata, H.; Tampo, H.; Matsubara, K.; Yamada, A.; Sakurai, K.; Ishizuka, S.; Niki, S.; Sakai, M. *Appl. Phys. Lett.* **2007**, *90*, 124104.
- Hill, M. R.; Russell, J. J.; Lamb, R. N. *Chem. Mater.* **2008**, *20*, 2461.
- Shan, F. K.; Liu, G. X.; Lee, W. J.; Shin, B. C. *J. Appl. Phys.* **2007**, *101*, 053106.
- Cong, G. W.; Wei, H. Y.; Zhang, P. F.; Peng, W. Q.; Wu, J. J.; Liu, X. L.; Jiao, C. M.; Hu, W. G.; Zhu, Q. S.; Wang, Z. G. *Appl. Phys. Lett.* **2005**, *87*, 231903.
- Kim, D. C.; Kong, B. H.; Jeon, S. Y.; Yoo, J. B.; Cho, H. K.; Park, D. J.; Lee, J. Y. *J. Mater. Res.* **2007**, *22*, 2032.
- Yang, C. -J.; Wang, S. -M.; Liang, S. -W.; Liang, S. -W.; Chang, Y. -H.; Chen, C.; Shieh, J. -M. *Appl. Phys. Lett.* **2007**, *90*, 033104.
- Vashei, Z.; Minegishi, T.; Suzuki, H.; Hanada, T.; Cho, M. W.; Yao, T.; Setiawan, A. *J. Appl. Phys.* **2005**, *98*, 054911.
- Bhattacharya, P.; Das, R. R.; Katiyar, R. S. *Appl. Phys. Lett.* **2003**, *83*, 2010.
- Yang, W.; Hullavarad, S. S.; Nagaraj, B.; Takeuchi, I.; Sharma, R. P.; Venkatesan, T.; Vispute, R. D.; Shen, H. *Appl. Phys. Lett.* **2003**, *82*, 3424.
- Chen, J.; Shen, W. Z. *Appl. Phys. Lett.* **2003**, *83*, 2154.
- Wang, Y. G.; Lau, S. P.; Lee, H. W.; Yu, S. F.; Tay, B. K.; Zhang, X. H.; Hng, H. H. *J. Appl. Phys.* **2003**, *94*, 354.
- Kim, M.; Hong, Y. J.; Yoo, J.; Yi, G.-C.; Park, G.-S.; Kong, K.-J.; Chang, H. *Phys. Stat. Sol. (RRL)* **2008**, *2*, 197.
- Meyer, B. K.; Alves; Hofmann, H. D. M.; Kriegseis, W.; Forster, D.; Bertram, F.; Christen, J.; Hoffmann, A.; StraBburg, M.; Dworzak, M.; Haboeck, U.; Rodina, A. V. *Phys. Stat. Sol. (b)* **2004**, *241*, 231.
- Teke, A.; Ozgur, U.; Dogan, S.; Gu, X.; Morkoc, H.; Nemeth, B.; Nause, J.; Everitt, H. O. *Phys. Rev. B* **2004**, *70*, 195207.
- Pan, C. J.; Lin, K. F.; Hsu, W. T.; Hsieh, W. F. *J. Appl. Phys.* **2007**, *102*, 123504.
- Lorentz, M.; Kaidashev, E. M.; Rahm, A.; Nobis, Th.; Lenzner, J.; Wagner, G.; Spemann, D.; Hochmuth, H.; Grundmann, M. *Appl. Phys. Lett.* **2005**, *86*, 143113.
- Xing, Y. J.; Xi, Z. H.; Xue, Z. Q.; Zhang, X. D.; Song, J. H.; Wang, R. M.; Xu, J.; Song, Y.; Zhang, S. L.; Yu, D. P. *Appl. Phys. Lett.* **2003**, *83*, 1689.
- Liu, Z. W.; Ong, C. K.; Yu, T.; Shen, Z. X. *Appl. Phys. Lett.* **2006**, *88*, 053110.
- Wang, R. P.; Xu, G.; Jin, P. *Phys. Rev. B* **2004**, *69*, 113303.
- Wassner, T. A.; Laumer, B.; Maier, S.; Laufer, A.; Mayer, B. K.; Stutzmann, M.; Eickhoff, M. *J. Appl. Phys.* **2009**, *105*, 023505.